Available online at https://doi.org/10.36303/SATNT.2021cosaami.08
Conference of the South African Advanced Materials Initiative

Determination of the dominant failure mechanism of P92 steam piping subjected to daily operational cycle using finite element (FE) technique

S Salifu[a*], D Desai[a], S Kok[b]

[a] *Department of Mechanical and Mechatronics Engineering, Tshwane University of Technology, Pretoria, South Africa*
[b] *Department of Mechanical and Aeronautical Engineering, University of Pretoria, Pretoria, South Africa*

Abstract

In a bid to minimise the cost of electrical energy production through the reduction in the quantity of coal usage, the power generation companies resolved to operate different daily cycles characterized by peak and off-peak energy demand periods. These daily operational cycles have left the power plant components operating in a possible creep-fatigue regime. As such, earlier failure of the plant's components such as the steam pipes due to creep, fatigue, or the combination of both failure modes became inevitable. This study employed finite element (FE) technique to determine the dominant failure mechanism and useful life of P92 power generation steam piping subjected to one of the daily operational cycles. The outcome of the study showed that the failure of the piping when subjected to the daily cycle is creep dominated, and failure due to fatigue or possible creep-fatigue interaction was impossible since the daily cycle was insufficient to induce the extensive plastic strain required for the initiation and propagation of fatigue failure. Hence, the best form of operating steam pipe/piping is steady-state, since subjecting them to daily cycles significantly reduce their useful life.

Keywords: Creep, stress relaxation, user subroutine, creep damage, useful life

1. Introduction

There is an unending call for the improvement in the production and generation of electrical energy while simultaneously reducing its cost of production. In this regard, the operating parameters like the temperature and pressure are altered, and the useful life of the plant's components are significantly influenced. The alteration of the operating parameters such as subjecting the components of the plants like the steam piping to daily operational cycles characterised by peak and off-peak periods left the component operating in the creep-fatigue regime. Hence, the unplanned failure of the component due to creep or fatigue or the combination of both failure mode becomes inevitable. Because power plant components such as the steam piping are subjected to high temperature and operating conditions, they are usually made of high creep resistant martensitic stainless steels such as X20 (12% Cr, 1% Mo, 0.25% V), P91 (9% Cr, 1% Mo) and P92 (9% Cr, 1.75% W, 0.5% Mo).

When considering the failure of a component that results from creep-fatigue interaction, the damage accumulated rate resulting from the complex loading cycles differ completely from those obtained by the linear summation of the damage rates produced by creep and the cyclic components.[1,2] If the failure of a component is characterized by creep-fatigue interaction, the manifestation of the fatigue part of the failure is characterized by the formation cracks while the creep part of the failure is characterized by cavitation damage in the form of creep voids at grain boundaries. Hence, the combination of fatigue damage and creep cavitation is found in a component whose failure is a result of creep-fatigue interaction, and an accelerated failure that exhibits a mixture of transgranular and intergranular paths[3] is observed.

Several studies have been conducted on components subjected to cyclic loading at elevated temperatures to determine the occurrence of failure due to creep-fatigue.[4-7] Despite the several types of researches conducted, there is still a strong controversy with regard to the failure mode, especially with steam pipes during an operation involving daily start-up and shutdown cycles.[8] Over the years, technological development has made the assessment of fatigue and creep behaviour possible numerically. Finite element (FE) techniques have been explored by researchers in the determination of the creep behaviour of high-temperature components[4,9,10] but there is limited use of this technique in the investigation of the possible failure of components like steam piping due to creep-fatigue interaction in the presence of simultaneous high-temperature and cyclic loading in the open literature.[3]

The absolute understanding of the damage evolution of components subjected to service in creep-fatigue environment is vital to the understanding and structural evaluation of the component's integrity in service.[11,12] Time fracture rules recommended by RCC-MR[13] and ASME BPV[14] standard have been used for analysing cyclic loading at elevated temperatures while R5 standard[15] recommends the use of ductility approach for the same operating conditions.

In this study, P92 martensitic stainless steel known for its excellent creep resistant properties and its use in power generation industries for the fabrication of steam pipes, is subjected to a steady-state power plant operating condition and operating condition characterised 24 hours daily cycle, aimed at reducing the cost of production. The 24 hours daily cycle consists of a total of 6 hours peak, 4 hours transient and 14 hours off-peak periods.[8] Finite element (FE) software Abaqus CAE/2020 alongside FE-Safe/Turbolife postprocessing software are employed to compute the

useful life and the dominant failure mode of the piping under the considered operating conditions.

2. Stresses developed in a steam pipe

Both mechanical and thermal stresses are developed in a thick-walled cylinder or pipe subjected to operation in a high-temperature environment. To compute the stress (mechanical) developed in a pipe (thick-walled), Lamé[16] developed mathematical expressions as shown below:

$$\sigma_r = P\frac{r_i^2(r^2-r_o^2)}{r^2(r_o^2-r_i^2)} \quad (1)$$

$$\sigma_t = P\frac{r_i^2(r^2+r_o^2)}{r^2(r_o^2-r_i^2)} \quad (2)$$

$$\sigma_z = \frac{P_i r_i^2}{r_o^2-r_i^2} \quad (3)$$

The effective stress (mechanical), σ_m in the pipe is computed using von-Mises theory as:

$$\sigma_m = \sqrt{[\sigma_t^2+\sigma_r^2+\sigma_z^2-(\sigma_t\sigma_r+\sigma_t\sigma_z+\sigma_r\sigma_z)]} \quad (4)$$

Using the expression in Eq. 5-7, the thermal stress developed in pipes at elevated temperatures,[17,18] is computed

$$\sigma_{tT} = \frac{\alpha E}{(1-v)r^2}\left[\frac{r^2+r_i^2}{r_o^2-r_i^2}\int_{r_i}^{r_o} Trdr - \int_{r_i}^{r} Trdr - Tr^2\right] \quad (5)$$

$$\sigma_{rT} = \frac{\alpha E}{(1-v)r^2}\left[\frac{r^2-r_i^2}{r_o^2-r_i^2}\int_{r_i}^{r_o} Trdr - \int_{r_i}^{r} Trdr\right] \quad (6)$$

$$\sigma_{zT} = \frac{\alpha E}{(1-v)}\left[\frac{2}{r_o^2-r_i^2}\int_{r_i}^{r_o} Trdr - T\right] \quad (7)$$

and the effective therml stress is obtained using von-Mises theory as shown below:

$$\sigma_T = \sqrt{[\sigma_t^2+\sigma_r^2+\sigma_z^2-(\sigma_t\sigma_r+\sigma_t\sigma_z+\sigma_r\sigma_z)]} \quad (8)$$

where,

σ_r, σ_t and σ_z represents the radial, circumferential and axial mechanical stress respectively, and σ_{rT}, σ_{tT} and σ_{tT} represents the thermal radial, circumferential axial stress respectively. σ_m and σ_T are the mechanical and thermal von-Mises stress.

Finally, the consequential thermomechanical stress, σ_{TM} induced in the pipe (straight) at elevated temperature is obtained by summing the effective mechanical and thermal stresses.

$$\sigma_{TM} = \sigma_m + \sigma_T \quad (9)$$

2.1 Creep-fatigue model

A constitutive creep model that assumes the minimum creep rate to be the summation of the linear and power law stress function was formulated[19] such that the diffusion creep mechanisms and the power law involve different defects which may be assumed independently before adding their creep rates as shown below. The formulated creep expression is able to account for low and high stresses similar to those experienced in the power generation industries, and it also describes effectively the minimum creep rate for advanced steels.[20,21]

$$\dot{\varepsilon}^{cr} = \varepsilon_p(T)\frac{\sigma}{\sigma_0(T)} + \varepsilon_p(T)\left(\frac{\sigma}{\sigma_0(T)}\right)^n \quad (10)$$

where n represents the material constant, while $\varepsilon_p(T)$ and $\sigma_0(T)$ represents the Arrhenius temperature functions.

2.2 Model for creep damage

Ductility exhaustion theory assumes that local strain developed in a component when subjected to a high-temperature environment attains a critical ductility value which results in a forward crack propagation.[11,22] At failure, the ratio of the creep rate to creep strain is used to determine the creep strain damage as shown below.

$$d_{cr} = \frac{\varepsilon_{cr}}{\varepsilon_f^*} \quad (11)$$

where d_{cr} is creep damage rate, ε_{cr} is creep strain rate, and ε_f^* is multiaxial creep failure strain.

The failure of the component occurs when the summation of the individual creep damages equals 1.

2.3 Fatigue damage model

Since the daily cycle of the steam piping under the stated service conditions will only amount to low cycle fatigue, the low cycle fatigue of the pipe is computed using the already established thermodynamic principle of low cycle fatigue[1,23], given as:

$$\frac{d_f}{dN} = \frac{R_v}{\varphi(1+\gamma)}\frac{(\Delta p)^{1+\gamma}}{(1-\omega)^{\alpha_0}} \quad (12)$$

where α_0, γ and φ represent material constants, R_v is the effect due to stress triaxiality, d_f represents damage due to fatigue, Δp represents the accumulated plastic strain in one cycle, and can be obtained with the Ramberg-Osgood equation:[4,24]

$$\frac{\Delta\sigma_e}{2} = K'\left(\frac{\Delta p}{2}\right)^{n'} \quad (13)$$

where K′ and n′ are material constants, while the equivalent or effective stress variation in one complete cycle is represented by $\Delta\sigma_e$.

2.4 Creep-fatigue interaction

Lagneborg[25] proposed an expression for the determination of the damage resulting from creep-fatigue interaction as shown below.

$$d_{cf} = b\left((d_f/dN)(d_c/dN)\right)^{1/2} \quad (14)$$

where, d_{cf} represents the damage due to creep-fatigue interaction, b represents the coefficient of creep-fatigue interaction, d_f/dN represents the damage due to fatigue after one cycle as depicted

in Equations (12)-(13) while $d_c dN$ represents the creep damage accumulated in one cycle. Hence, Equation. (11) is expressed as

$$\frac{d_c}{dN} = \int_0^{t_h} d_c dt \quad (15)$$

where, $_h$ is one complete cycle hold time. Hence, the expression for the creep-fatigue interaction damage model is given as

$$\frac{d_{cf}}{dN} = \frac{d_c}{dN} + \frac{d_f}{dN} + b\left(\left(\frac{d_c}{dN}\right)\left(\frac{d_f}{dN}\right)\right)^{1/2} \quad (16)$$

3. Finite element model

The three-dimensional model (3D) of the pipe-insulation assembly was developed in Abaqus/CAE 2020 such that the real dimensions of a typical steam pipe and insulation jacket was captured. Figure 1 shows the assembly model of the pipe and insulation jacket, while Table 1 shows their dimensions.

Since the creep stress developed has no significant influence on the distribution of temperature in the pipe/piping, the analysis was carried out sequentially with the heat transfer analysis first, then the creep analysis.[30] Appropriate mechanical boundary conditions which allow the assembly was able to be displaced in V_1, V_2 and V_3 direction and undergo rotation in V_{R1}, V_{R2} and V_{R3} direction as shown in Figure 2(a) was applied.

As depicted in Figure 2(b), a seed size of 50 mm was discovered to be appropriate for both the heat transfer and creep analysis after conducting mesh convergence studies. "An operating temperature of 550ºC having 10 000 W/m²K convection heat transfer coefficient[31] was applied to the interior surface of the pipe while 25ºC temperature having 18.0 W/m²K convection heat transfer coefficient was applied to the exterior surface of the insulation jacket in the assembly".[28,32]

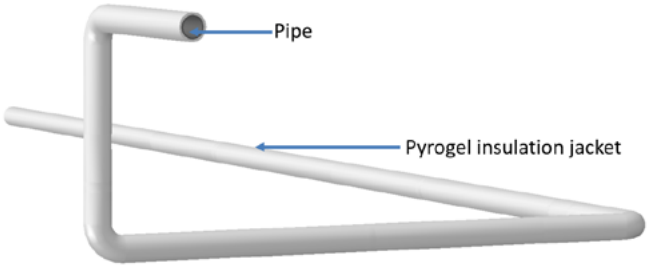

Figure 1: Assembly model of pipe and insulation jacket

A steam pressure load of 18.0 MPa representing the optimal operating pressure of the piping was applied to the interior surface of the pipe in the steady-state creep analysis while the steam pressure and temperature profile representing the different sections of the daily cycle was applied to the pipe in the analysis involving cycle. Figure 3(a) shows the material properties of the steel pipe which have 0.33 Poisson ratio and 33.0 W/mK thermal conductivity while Figure 3(b) shows the steam pressure and temperature at the different sections of the daily cycle. From Figure 3(b), the maximum operating pressure (18.0 MPa) was maintained at peak while the pressure dropped to 0.1 MPa during the off-peak periods.

Through curve fitting of the P92 steel creep data obtained experimentally, the constitutive creep model constants were obtained as shown in Table. 2. After which script for the creep model was written in Fortran and executed in Abaqus CAE/2020 to determine the creep strain, stress and stress relaxation of the piping. Also, the creep damage, creep damage accumulation and the pipe's useful life were computed using fe-safe/Turbolife software, with the effect of stress relaxation fully incorporated in the analysis. The steam pipe was presumed to have machined-finish surface with surface roughness $16 < Ra \leq 40$ µm, and ductility exhaustion technique with morrow was used in the analysis

4. Results and discussions

A plot showing the temperature distribution across thickness of the piping when it was subjected to steady-state analysis is shown in Figure 3. From the figure, it was discovered that the optimal applied operating temperature was maintained inside the piping, while the considerably low temperature value (42.9 ºC) developed on the insulation jacket signifies that the piping is well-insulated, and the characteristic low temperature value obtained on the surface

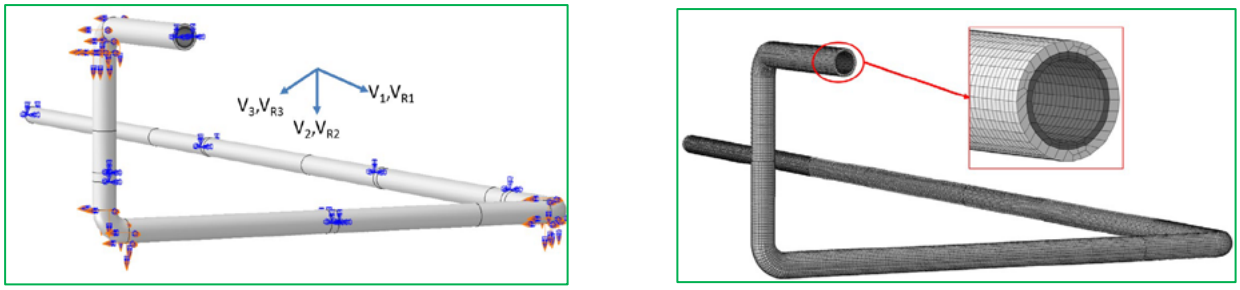

(a) (b)

Figure 2: Applied (a) boundary conditions and (b) pipe-insulation assembly mesh

Table 1: Steel pipe and pyrogel insulation jacket dimensions[26-29]

Materials	Length (m)	Diameter (m)		Elbow Radius (m)	Thickness (m)
		Internal	External		
Pipe	52.10	0.38	0.44	0.50	0.03
Insulation Jacket	52.10	0.44	0.54	0.50	0.05

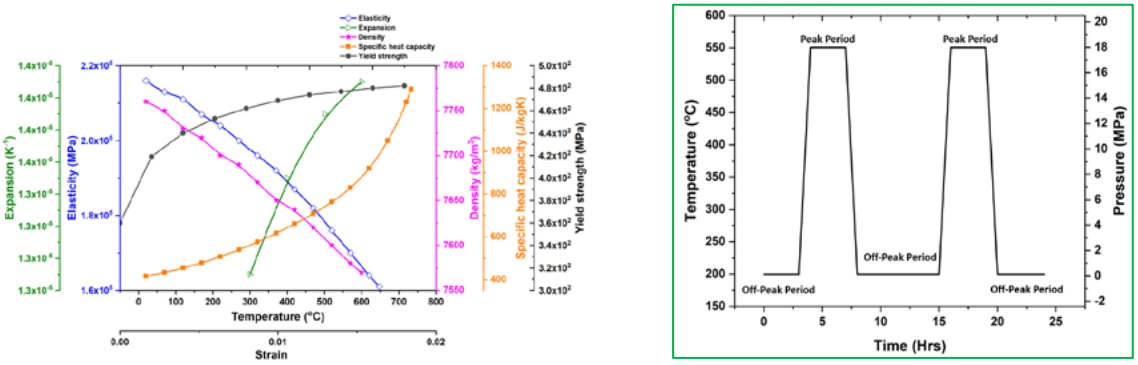

(a) (b)

Figure 3: (a) P92 material properties[29,33] and (b) 24-hours operational cycle

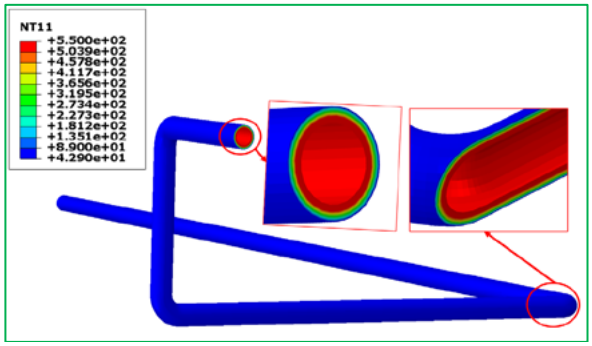

Figure 3: Temperature distribution plot

(outer) of the jacket buttresses the fact that pyrogel is indeed a good insulation jacket for high-temperature components.[35]

The plot for the creep stress and strain of the piping after one hour of steady-state analysis is shown in Figure 4(a) and (b) while the creep stress and strain after an hour of steady-state operation at the straight section of the piping is depicted in Figure 5. From the plots, it was discovered that the optimum creep stress (206.3 MPa) and strain (2.833×10^{-4}) was developed at the intrados of the elbows in the piping. Thus, making this region of the piping more prone to

Table 2: P92 steel creep constants for the used model at 550°C[34]

$\varepsilon_p(T)$ ($\times 10^{-8}$ h^{-1})	$\sigma_0(T)$ ($\times 10^8$ Pa)	n
2.145	1.284	17.929

failure. Figure 6 shows the creep stress and strain at failure when the piping was subjected to steady-state analysis and the analysis characterised by daily cycle. At failure, the maximum creep stress and strain are developed at the intrados of the piping just like that obtained in the steady-state analysis. However, the contour plot of the maximum stress and strain becomes obvious at the outer of the elbows. In both analyses (steady-state and the analysis involving daily cycle), the extensive plastic strain required for the initial and propagation fatigue crack was not observed. Hence, failure due to fatigue or creep-fatigue interaction is impossible.

Creep damage and the useful life plot of the P92 steam piping under the two operating conditions understudy is depicted in Figure 7. It was observed from the plot that the steady-state analysis survived a useful creep life of 21.31 years with creep damage of 5.361×10^{-6} at failure, while the analysis with cycles survived a creep life of

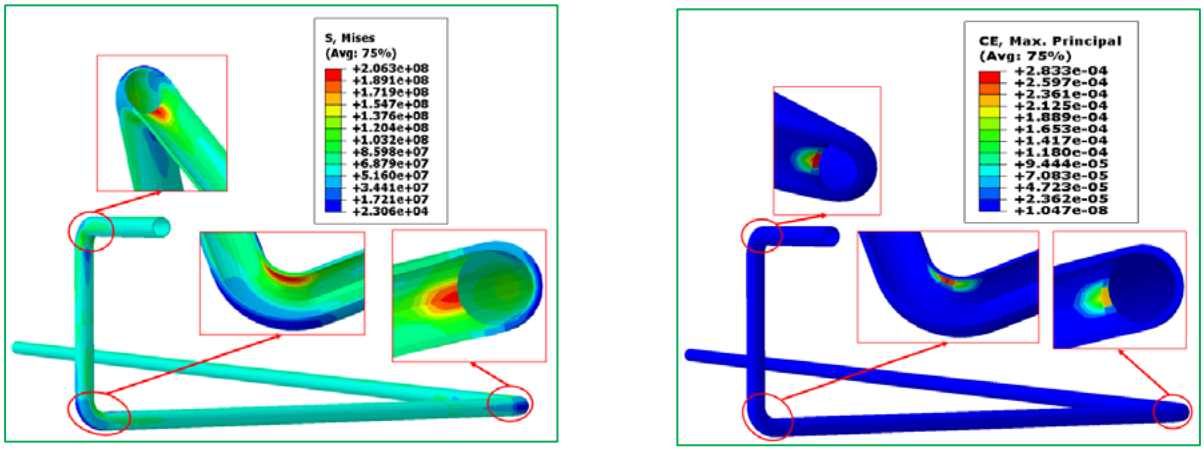

(a) (b)

Figure 4: Contour plot for creep (a) stress and (b) strain

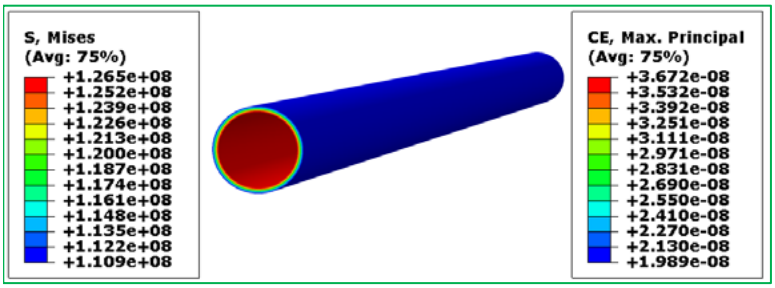

Figure 5: Result of distribution of creep stress and strain at the straight section of the piping

8.88 years with creep damage of 1.286×10^{-5} at failure. Similar to the creep stress and strain, the worst damage and creep life in both analyses were obtained at the intrados of the piping. This further buttress the fact that failure of steam piping in the creep or creep-fatigue regime would initiate from the intrados of the piping.

To determine the possibility of failure resulting from creep-fatigue interaction, the steady-state analysis and analysis involving daily cycle output database result was post-processed in fe-safe/Turbolife software, and the outcome further confirmed that the steam piping cannot fail due to creep-fatigue interaction since the required plastic strain needed for such to occur was not induced. Figure 8 is a plot obtained from the analysis conducted using fe-safe/Turbolife software and the plot shows that the failure of the piping is mainly due to creep alone.

For components operated in creep regime, the developed stress are known to relax with an increase in the time of operation. Depicted in Figure 9(a) is the creep strain and stress relaxation pattern of the steam piping when subjected to steady-state operation, and operation involving daily cycle. From the plot, it was observed that the piping subjected to steady-state analysis experiences a faster stress relaxation with a much higher creep strain at every time increment. The difference in the characteristic stress relaxation and developed creep strain behaviour observed is attributed to the amount of time spent by the piping in both analyses at high-temperature creep regime. The stress relaxation in the steady-state analysis is faster and its creep strain is higher because the piping spent its entire duration in the high-temperature condition while the analysis involving daily cycle spent only a fraction of its entire duration in the high-temperature environment. Nevertheless, the evolution of creep damage in both analyses shows that faster creep damage accumulation occurs in the analysis involving daily operational cycles because of its constant operation at higher stresses. Depicted in Figure 9(b) is the accumulation of creep damage for both analyses prior to failure. The accumulation of the creep damage with daily cycle reached 1 (failure) after 77 788

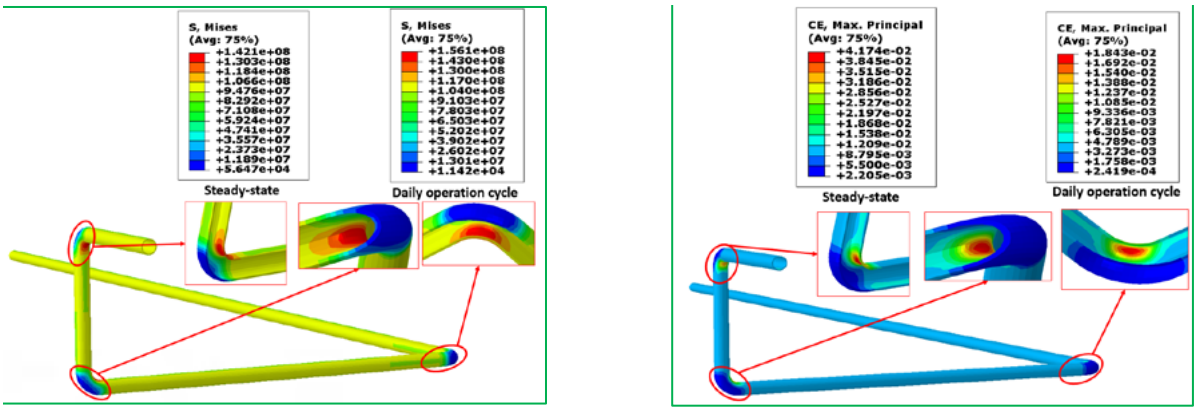

Figure 6: Developed creep (a) stress and (b) strain at failure for the two operating conditions

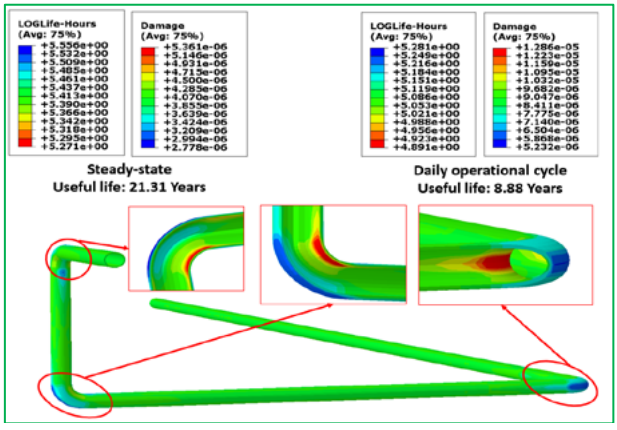

Figure 7: Creep damage and useful life of piping at steady-state and creep analysis with cycle

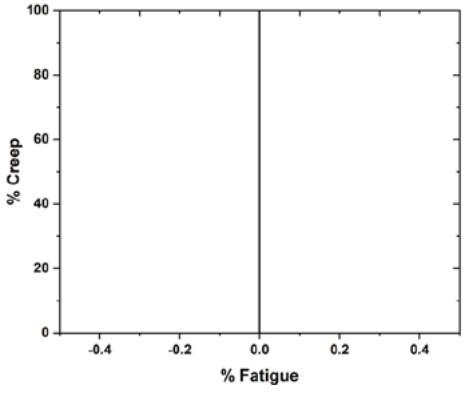

Figure 8: Plot showing creep as the only mode of failure

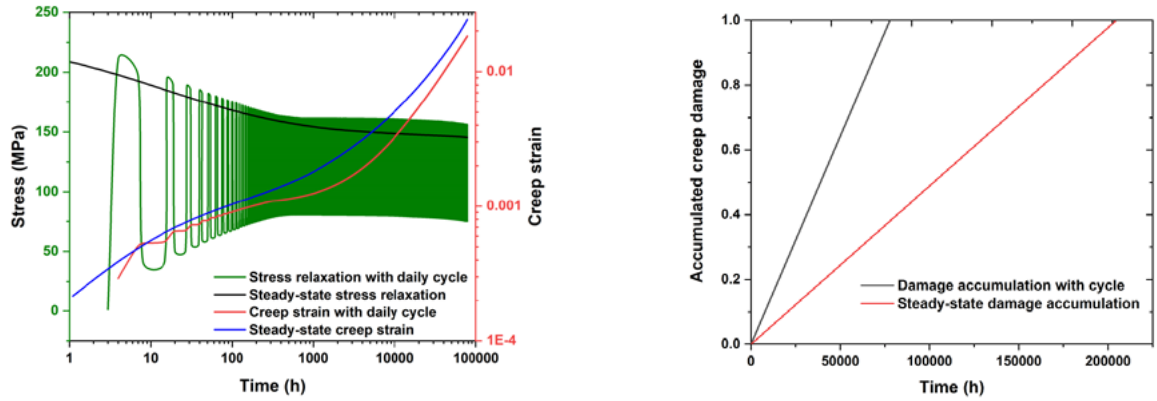

Figure 9: (a) Stress relaxation and creep strain, and (b) creep damage accumulation

Table 3: % deviation between analytical and simulated creep strain of a straight section of the piping

Calculated		FE simulated		% Deviation
Stress (MPa)	Strain strain	Stress (MPa)	Strain strain	
126.78	37.56×10^{-9}	126.50	36.72×10^{-9}	2.24

hours while the analysis subjected to steady-state reached 1 after 186 675 hours of operation.

4.1 Validation of creep strain

Steam piping networks are characterized by complex shapes which makes the validation of the creep strain in the entire piping practically impossible. Nevertheless, the thermo-mechanical stress developed in the straight section of the piping can be computed using Lame's equations for the mechanical stress in thick-walled pipes while the thermal stress is computed using the expressions for the thermal stress in straight pipes after which the effective thermo-mechanical stress is obtained and substituted into the equation for the constitutive creep model to determine the developed analytical creep strain in the straight section of the piping after one hour of steady-state operation. Shown in Table 3 is the analytically computed and FE simulated creep strain at the straight section of the piping. From the table, it is observed that a good correlation exists between the calculated and simulated creep strain of the pipe.

5. Conclusion

FEA of steam piping fabricated from P92 steel and subjected to two different operating conditions was simulated in Abaqus to determine the dominant failure mode. The temperature distribution profile, creep stress, creep strain and stress relaxation pattern developed in the piping was determine using Abaqus CAE/2020, while the useful life, creep damage, creep damage accumulation and the possibility of the failure of the piping due to creep-fatigue interaction was determined using fe-safe/Turbolife software. The results of the analyses show that the failure of the steam pipe under the two operating conditions considered (steady-state and analysis with daily cycle) is due to creep alone as both analyses lacked the required plastic strain needed to induce fatigue crack. In addition, the maximum creep stress, strain, worst creep life and damage was located on the intrados of the elbows in both analyses. Furthermore, the analysis involving daily cycle gave the worst creep life and damage because of the faster creep damage accumulation that results from the higher stresses in operation during the analysis. Finally, a good correlation was achieved when the calculated and FE simulated creep strain at the straight section of the steam pipe were compared, as the percentage deviation between the two creep strain is within the acceptable 0-10% range for engineering components.

Acknowledgement

This research has been profusely supported by Tshwane University of Technology and the University of Pretoria, South Africa. Also, the authors greatly appreciate the unending support of Eskom Power Plant Engineering Institute (Republic of South Africa).

References

1. X. Zhang, S.-T. Tu, and F. Xuan, "Creep–fatigue endurance of 304 stainless steels," *TheoreticalApplied Fracture Mechanics,* vol. 71, pp. 51-66, 2014.
2. R. Hales, "A quantitative metallographic assessment of structural degradation of type 316 stainless steel during creep-fatigue," *Fatigue Fracture of Engineering Materials Structures,* vol. 3, no. 4, pp. 339-356, 1980.
3. S. Salifu, D. Desai, and S. Kok, "Creep–fatigue interaction of P91 steam piping subjected to typical start-up and shutdown cycles," *Journal of Failure Analysis and Prevention,* 2020.
4. H. Jing, D. Su, L. Xu, L. Zhao, Y. Han, and R. Sun, "Finite element simulation of creep-fatigue crack growth behavior for P91 steel at 625° C considering creep-fatigue interaction," *International Journal of Fatigue,* vol. 98, pp. 41-52, 2017.
5. K. Sadananda and P. Shahinian, "Effect of environment on crack growth behavior in austenitic stainless steels under creep and fatigue conditions," *Metallurgical transactions A,* vol. 11, no. 2, pp. 267-276, 1980.
6. J.-F. Wen, S.-T. Tu, X.-L. Gao, and J. Reddy, "Simulations of creep crack growth in 316 stainless steel using a novel creep-damage model," *Engineering fracture mechanics,* vol. 98, pp. 169-184, 2013.
7. B. Fournier *et al.*, "Creep–fatigue–oxidation interactions in a 9Cr–1Mo martensitic steel. Part I: Effect of tensile holding period on fatigue lifetime," *International Journal of Fatigue,* vol. 30, no. 4, pp. 649-662, 2008.
8. S. Salifu, D. Desai, and S. Kok, "Numerical investigation of creep-fatigue interaction of straight P91 steam pipe subjected to start-up and shutdown cycles," *Materials Today: Proceedings,* 2020.

9. Z. Ding, Z. Gao, X. Wang, and Y. Jiang, "Modeling of fatigue crack growth in a pressure vessel steel Q345R," *Engineering Fracture Mechanics,* vol. 135, pp. 245-258, 2015.
10. H. Li, H. Yuan, and X. Li, "Assessment of low cycle fatigue crack growth under mixed-mode loading conditions by using a cohesive zone model," *International Journal of Fatigue,* vol. 75, pp. 39-50, 2015.
11. L. Xu, L. Zhao, Z. Gao, and Y. Han, "A novel creep–fatigue interaction damage model with the stress effect to simulate the creep–fatigue crack growth behavior," *International Journal of Mechanical Sciences,* vol. 130, pp. 143-153, 2017.
12. M. Chrzanowski, "Use of the damage concept in describing creep-fatigue interaction under prescribed stress," *International Journal of Mechanical Sciences,* vol. 18, no. 2, pp. 69-73, 1976.
13. R.-M. J. Z. P. A. Code, "Design and Construction Rules for Mechanical Components of FBR Nuclear Islands and High Temperature Applications, Appendix A16, Tome I, vol," 2007.
14. A. Boiler, *Rules for Construction of Pressure vessels*. American Society of Mechanical Engineers, 2013.
15. R. J. B. E. G. L. Ainsworth, "R5: Assessment procedure for the high temperature response of structures," vol. 3, 2003.
16. B. Kanlıkama, A. Abuşoğlu, and İ. H. Güzelbey, "Coupled thermoelastic analysis of thick-walled pressurized cylinders," *International Journal of Energy and Power Engineering,* vol. 2, no. 2, pp. 60-68, 2013.
17. A. Kandil, A. El-Kady, and A. El-Kafrawy, "Transient thermal stress analysis of thick-walled cylinders," *International journal of mechanical sciences,* vol. 37, no. 7, pp. 721-732, 1995.
18. V. Pesonen, "Online Creep and Fatigue Monitoring in Power Plants," 2014.
19. K. Naumenko, H. Altenbach, and A. Kutschke, "A constitutive model for creep and long-term strength in advanced heat resistant steels and structures," *Journal of Transition,* vol. 2, no. 3, p. 4, 2009.
20. L. Kloc and V. Sklenička, "Confirmation of low stress creep regime in 9% chromium steel by stress change creep experiments," *Materials Science and Engineering: A,* vol. 387, pp. 633-638, 2004.
21. K. Naumenko and Y. Kostenko, "Structural analysis of a power plant component using a stress-range-dependent creep-damage constitutive model," *Materials Science and Engineering: A,* vol. 510, pp. 169-174, 2009.
22. R. Skelton and D. Gandy, "Creep–fatigue damage accumulation and interaction diagram based on metallographic interpretation of mechanisms," *Materials at High Temperatures,* vol. 25, no. 1, pp. 27-54, 2008.
23. J. Lemaitre and A. Plumtree, "Application of damage concepts to predict creep-fatigue failures," *Journal of Engineering Materials,* vol. 101, no. 3, pp. 284-292, 1979.
24. W. Ramberg and W. R. Osgood, "Description of stress-strain curves by three parameters," *NTRS - NASA Technical Reports Server,* 1943.
25. R. Lagneborg and R. Attermo, "The effect of combined low-cycle fatigue and creep on the life of austenitic stainless steels," *Metallurgical transactions A,* vol. 2, no. 7, pp. 1821-1827, 1971.
26. T. Rasiawan, "The influence of prior creep damage on the fracture localisation in X20 CrMoV12-1 cross-weld creep tests," Master's Dissertation, University of Cape Town, 2017.
27. Pyrogel-XTE-Datasheet, "High-Performance Aerogel Insulation for Industrial and Commercial Applications."
28. S. Salifu, D. Desai, S. Kok, and O. J. P. M. Ogunbiyi, "Thermo-Mechanical Stress Simulation of Unconstrained Region of Straight X20 Steam Pipe," vol. 35, pp. 1330-1336, 2019.
29. S. Salifu, D. Desai, and S. Kok, "Influence of Diverse Operating Cycles on the Useful Creep Life of P92 Steam Piping," *Journal of Failure Analysis and Prevention,* pp. 1-10, 2021.
30. S. D. Systemes, "ABAQUS 6.13 User's manual," *Dassault Systems, Providence, RI,* 2013.
31. S. Salifu, D. Desai, F. Fameso, O. Ogunbiyi, S. Jeje, and A. Rominiyi, "Thermo-mechanical analysis of bolted X20 steam pipe-flange assembly," *Materials Today: Proceedings,* 2020.
32. S. Salifu, D. Desai, and S. Kok, "Comparative evaluation of creep response of X20 and P91 steam piping networks in operation," *The International Journal of Advanced Manufacturing Technology,* vol. 109, no. 7, pp. 1987-1996, 2020.
33. JAHM-Software. Temperature Dependent Material Properties Database, MPDB [Online]. Available: https://www.jahm.com/
34. P. Kral *et al.*, "The effect of ultrafine-grained microstructure on creep behaviour of 9% Cr steel," *Materials,* vol. 11, no. 5, p. 787, 2018.
35. S. Salifu, D. Desai, and S. Kok, "Numerical simulation and creep-life prediction of X20 steam piping," *Materials Today: Proceedings,* 2020.